# Middle Triassic lake deepening in the Ordos Basin of North China linked with global sea-level rise

Xin Jin [a,*], Viktória Baranyi [b], Marcello Caggiati [c], Marco Franceschi [d], Corey J. Wall [e], Guanglin Liu [f], Mark D. Schmitz [e], Piero Gianolla [c], James G. Ogg [a,g], Gang Lu [a], Zhiqiang Shi [a,*], Nereo Preto [h]

[a] State Key Laboratory of Oil and Gas Reservoir Geology and Exploitation, Chengdu University of Technology, Chengdu, Sichuan 610059, China
[b] Department of Geology, Croatian Geological Survey, Sachsova 2, P.O. Box 268, HR-10000 Zagreb, Croatia
[c] Department of Physics and Earth Sciences, Università degli Studi di Ferrara, Via Saragat, 1, Ferrara 44100, Italy
[d] Department of Mathematics and Geosciences, Università degli Studi di Trieste, via Edoardo Weiss, 2, 34128 Trieste, Italy
[e] Department of Geosciences, Boise State University, 1910 University Drive, Boise, ID 83725-1535, USA
[f] Exploration and Development Research Institute, Changqing Oilfield Company of PetroChina, Xi'an 710018, China
[g] State Key Laboratory of Biogeology and Environmental Geology and School of Earth Sciences, China University of Geosciences, Wuhan 430074, China
[h] Dipartimento di Geoscienze, Università degli Studi di Padova, Via G. Gradenigo 6, Padova, Italy

ARTICLE INFO

Editor: Dr Maoyan Zhu

*Keywords:*
Yanchang formation
Chang 7 Member
Ladinian
CA-ID-TIMS
Carbon isotopes
Lacustrine

ABSTRACT

The Yanchang Formation was deposited during the Middle Triassic in a vast lacustrine basin in the modern Ordos Basin and is a main target for hydrocarbon exploration in Central China. It is divided, based on sedimentary cycles and lithology, into the Chang 10 (the oldest) to Chang 1 (the youngest) members. During the deposition of the Chang 7 Member, the Ordos lake system reached its maximum depth and large volumes of organic-rich sediments were deposited. The evolution of the Ordos Basin sedimentary system during this phase is, however, not completely understood, and uncertainty still exists as for the chronostratigraphy of Chang 7 Member. We acquired palynological markers and palynofacies and a high-resolution $\delta^{13}C_{org}$ record through the entire Chang 7 Member, and a ID-TIMS $^{206}Pb/^{238}U$ date of 240.95 ± 0.033 Ma from a volcanic ash bed in the middle of this Member. These imply that the maximum deepening phase of the lacustrine system was during the earliest Ladinian. Evidence of marine influence in the Ordos Basin at that time and comparison to the sea-level oscillations observed in Western Tethys suggest that a global eustatic rise and highstand may have played a role in determining lake-level variations.

## 1. Introduction

Intracratonic basins with terrestrial sediments are a challenge for chronostratigraphy. Pollen, spores, plants, fresh-water or brackish-water invertebrates, and continental vertebrate remains may be found, but usually these have far lower stratigraphic resolution and an uncertain correlation to marine index fossils, such as ammonoids and conodonts.

The Ordos Basin, the second largest petroliferous basin of China, was a continental intracratonic basin through the Mesozoic (e.g., Liu et al., 2013; Bai and Ma, 2020). The Yanchang Formation is characterized by deep-water to shallow lacustrine facies associations and hosts tight oil source rocks and super-low permeability reservoirs (Yang et al., 2005; Yang et al., 2013; Lin et al., 2017; Bai and Ma, 2020). As a consequence of its economic relevance, numerous boreholes have been drilled through the Yanchang Formation. The sedimentary succession of the Yanchang Formation displays cyclic facies changes that manifest the expansions and contractions of a large lacustrine system and has been divided in ten members from Chang 10 (the oldest) to Chang 1 (the youngest) (Zou et al., 2010; Yang and Deng, 2013). One of the main challenges with the Yanchang Formation has been resolving precise ages and time spans of the different members, and this hinders the understanding of its sedimentary and paleo-environmental evolution within a larger context.

Palynological and other biostratigraphic data (plants, bivalves, ostracods, vertebrate and invertebrate fossils) assign the Yanchang

* Corresponding authors.
*E-mail addresses:* jinxin2012cdut@163.com (X. Jin), szqcdut@163.com (Z. Shi).

Accepted 28 September 2021

Formation to the Middle to Late Triassic (Deng et al., 2018 and reference therein). Volcanic zircons from multiple ash beds at various stratigraphic horizons have been dated by different U/Pb methods. Yang and Deng (2013) reported a Late Triassic age (up to 222.2 ± 2.0 Ma) for the Chang 7 Member based on LA-ICP-MS (Laser Ablation Inductively Coupled Plasma Mass Spectrometry) analysis on zircons. In contrast, biostratigraphic ages and radiometric dates obtained through ID-TIMS (Isotope Dilution Thermal Ionization Mass Spectrometry) assign the Chang 7 Member to the Middle Triassic (Deng et al., 2018; Zhu et al., 2019). A recent U—Pb dating of zircons on tuff layers in outcrops of the Yanchang Formation yielded ages ranging from 234 to 236 Ma for the Chang 7 Member (Sun et al., 2020). Independent cyclostratigraphic analyses of Chang 7 Member by Chen et al. (2019) and Zhang et al. (2019b) provided a floating astrochronological time scale that implied that this member, alone, spans ca. 5 to 7 Myr. These discrepancies clearly indicate that additional accurate age determinations and constraints are needed to provide a precise chronostratigraphy for the Yanchang Formation and its organic-rich Chang 7 Member before one can interpret the evolution of the Ordos lake system.

In this study, we obtained a high-precision U—Pb (CA-ID-TIMS) date on zircons, palynological data and a high-resolution organic carbon isotope record from a continuous cores through the Chang 7 Member. These new age constraints allow an improved chronostratigraphy for the Chang 7 Member and for the timing of its main facies changes. These also enable a comparison to marine-based chronostratigraphy and suggest potential links between the oscillations of sea-level and of lake-level during the Middle Triassic.

## 2. Geological setting

During the Middle and Late Triassic, the North China Plate had accreted to the northeastern part of the Pangaea mega-continent. The Ordos Basin, a large multicycle cratonic basin (Yang et al., 2005) with an area of about $32 \times 10^4$ km$^2$, occupied the western portion of North China Plate since the Late Permian. During the Triassic, it was located at ca. 30° N latitude in a temperate to subtropical climate belt (Fig. 1A; Ji et al., 2010). The modern Ordos Basin is bordered by the Yinshan Mountain to the north, Taihang Mountain to the east, the Qinling orogenic belt to the south, and the western Ordos thrust belt to the west (Fig. 1B) (Sun et al., 1989; Darby and Ritts, 2002; Ritts et al., 2004).

During the Middle to Late Triassic, the collision between North China and South China blocks resulted in the closure of the relicts of Youjiang and Qinling troughs and the formation of the Qinling Mountains (Li et al., 1993; Liu et al., 2013; Dong et al., 2015 and references therein). As a result, the southern Ordos Basin was involved in tectonic activity, and there was differential subsidence of its internal regions (Deng et al., 2013; Yang and Deng, 2013; Liu et al., 2013; Gao et al., 2020 and references therein). During this time, fluvial-lacustrine-deltaic sediments deposited the 1300 m thick succession of the Yanchang Formation (Fig. 1C, D) (e.g., Zou et al., 2010; Yang and Deng, 2013; Deng et al., 2018).

The Yanchang Formation lays disconformably over the Middle Triassic Zhifang Formation, and its top is eroded to different degrees, being unconformably overlain by the Lower Jurassic Yan'an Formation or by the Fuxian Formation depending on the locality (Fig. 1D) (e.g., Yang and Deng, 2013). The subdivision of the Yanchang Formation is still not standardized (summarized in the Deng et al., 2018), but the general concept is a subdivision of into numbered members from a lower Chang 10 to an uppermost Chang 1, according to the sedimentary facies and lithological associations (Fig. 1D) (Yang and Deng, 2013; Qiu et al., 2014; Deng et al., 2018). During the deposition of the Chang 7 Member, the lacustrine basin reached its maximum extent (Fig. 1D; Ji et al., 2010; Zou et al., 2010; Yang and Deng, 2013). The Chang 7 Member is further subdivided into three submembers or units based on lithofacies, from a lower Chang $7_3$ to an upper Chang $7_1$ (e.g., Zhang et al., 2019b; Sun et al., 2020).

## 3. Material and analytical methods

For our study, we selected a continuously cored interval from the borehole, Zheng 40 (Z40), located in the southern Ordos Basin (Fig. 1C). The core Z40 spans the Chang 7 Member and the lower part of Chang 6 Member, and the Chang 7 Member was further subdivided into Chang $7_3$, Chang $7_2$ and Chang $7_1$ submembers (Fig. 2). The lower submember of Chang $7_3$ is mainly consists of oil-rich shales with interbedded tuff layers at the bottom, and its upper part is composed of dark gray shales, fine-grained sandstones and siltstones. The overlying Chang $7_2$ and Chang $7_1$ submembers mainly consist of dark gray shales, shaly siltstones, siltstones and fine-grained sandstones with thin tuff intercalations (Fig. 2). We analyzed these units in Z40 for U—Pb zircon dating, for palynological composition and for carbon stable isotopes of organic matter. Three tuff layers were identified, and the middle one was selected for U—Pb geochronology analysis (Fig. 2). All the data are listed in the Supplementary dataset.

### 3.1. CA-ID-TIMS method

Prior to the ID-TIMS analysis, the zircon grains were extracted and photographed under reflected light and cathodoluminescence (CL). Sixty of these volcanic zircon grains were then ablated by the LA-ICP-MS (Fig. SF1, for raw data see Supplementary dataset). The detailed analytical processes and results are listed in Supplementary file (SF). Seven grains with dominant CL patterns and consistent in-situ LA-ICP-MS U—Pb dates were selected for further high-precision isotopic analysis. Individual zircon grains were plucked from epoxy mounts and placed in a muffle furnace at 900 °C for 60 h in quartz beakers to anneal minor radiation damage and prepare the crystals for subsequent chemical abrasion (Mattinson, 2005).

U—Pb geochronology methods for ID-TIMS follow those previously published by Davydov et al. (2010) and Schmitz and Davydov (2012). Zircon crystals were subjected to a modified version of the chemical abrasion method of Mattinson (2005), whereby single crystal fragments plucked from grain mounts were individually abraded in a single step with concentrated HF at 190 °C for 12 h. All analyses were undertaken on crystals previously mounted, polished and imaged by cathodoluminence (CL), and selected on the basis of zoning patterns. Zircon fragments were dissolved in Parr bombs at 220 °C for 48 h. Dissolved zircon solutions were subsequently dried, redissolved in 100 μl 6 N HCl, and converted to chlorides in Parr bombs at 180 °C for 12 h; after which, solutions were dried again and redissolved in 50 μl 3 N HCl. U and Pb were isolated by anion exchange column chromatography using 50 μl columns and AG-1 × 8 resin [200–400 mesh, chloride form (Eichrom); Krogh, 1973].

The U—Pb aliquot was loaded in a silica gel emitter (Gerstenberger and Haase, 1997) to an outgassed, zone-refined Re filament. Isotopic determinations were performed using an IsotopX PhoeniX-62 TIMS. A correction for mass-dependent Pb fractionation was applied based on repeated measurements of NBS 982 (Catanzaro et al., 1968) Pb on both the Daly ion counter [0.16 ± 0.03%) amu$^{-1}$; 1 *s*] and the Faraday cups [0.10 × (1 ± 0.02%) amu$^{-1}$; 1 *s*]. Uranium was run as an oxide ($UO_2$) and measured in static mode on Faraday detectors equipped with $10^{12}$ Ω resistors. The U mass fractionation for the same analyses was calculated using the $^{233}U/^{235}U$ ratio of the double spike solution (0.99506 ± 0.01%, 1 *s*).

U—Pb dates and uncertainties for each analysis were calculated using the algorithms of Schmitz and Schoene (2007) and the U decay constants of Jaffey et al. (1971), and a value of $^{238}U/^{235}U = 137.88$. Uranium oxide measurements were corrected for isobaric interferences using an $^{18}O/^{16}O$ value of 0.00206. Uncertainties are based upon non-systematic analytical errors, including counting statistics, instrumental fractionation, tracer subtraction, and blank subtraction. These error estimates should be considered when comparing our $^{206}Pb/^{238}U$ dates with those from other laboratories that used tracer solutions calibrated

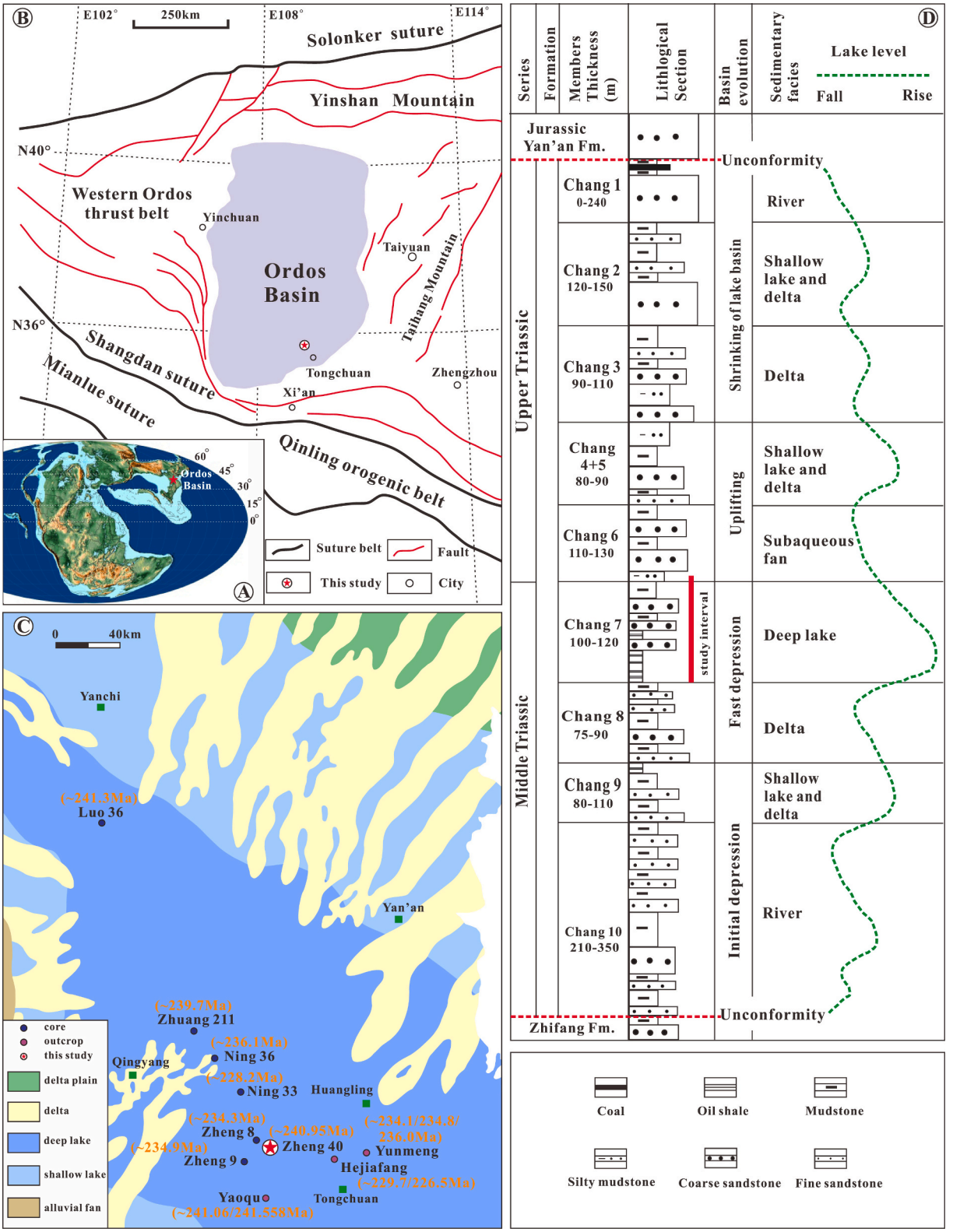


**Fig. 1.** A). General paleogeographic position of the Ordos Basin during the Late Triassic (Scotese, 2014). B). Tectonic units of the Ordos Basin (modified from Wang et al., 2014). C). Paleogeographic map of the sedimentary facies of the Chang 7 Member (modified from Chen et al., 2019) and the position of boreholes/outcrops of the lower portion of the Chang 7 Member that have yielded zircon dates by different methods (Deng et al., 2013; Wang et al., 2014; Zhang et al., 2014; Wang et al., 2017b; Zhu et al., 2019; Sun et al., 2020). Note: U—Pb date (this study) of Zheng 40 is from the middle portion of the Chang 7 Member. D). Lithology, depositional environments, and inferred lake-level fluctuations within the Yanchang Formation, and its contact relations with the underlying and overlying strata (modified from Yang et al., 2017).

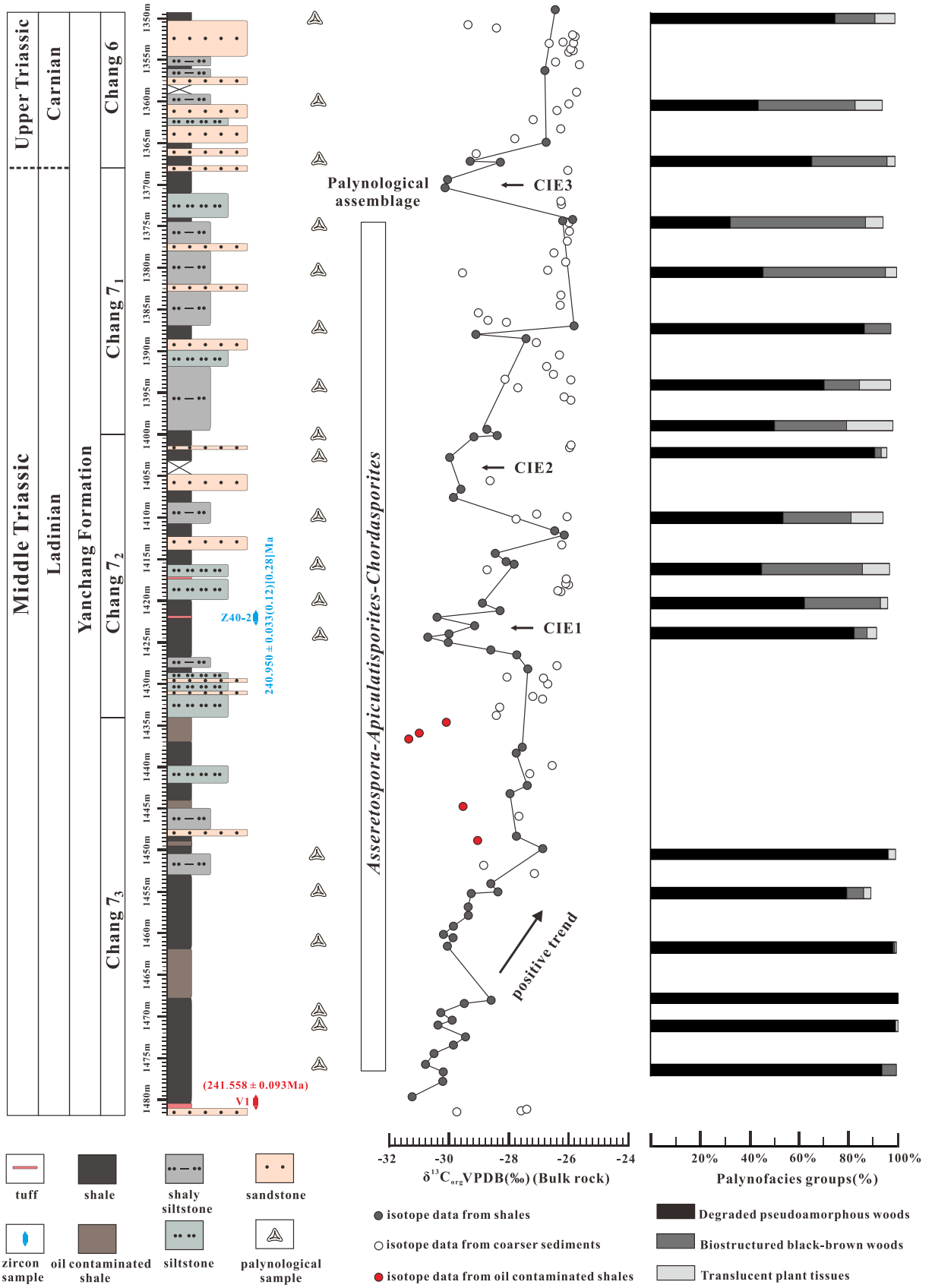


**Fig. 2.** Lithologic units, palynological assemblage zones, relative proportion of the palynofacies groups expressed as percentages (%), organic carbon isotopic curve of shales that are free from oil contamination (curve connecting black dots) and of other sediments, and horizon yielding the high-precision U—Pb zircon date (in blue font) from the Chang 7 Member of core Z40. Note that only the most frequent palynofacies groups are plotted (total counts are available in the Supplementary dataset). The ID-TIMS date from zircons of the V1 volcanic ash sample at the Yishi Village (in red font at bottom) is from Zhu et al. (2019). (For interpretation of the references to colour in this figure legend, the reader is referred to the web version of this article.)

against the EARTHTIME gravimetric standards. When comparing our dates with those derived from other decay schemes (e.g., $^{40}Ar/^{39}Ar$, $^{187}Re—^{187}Os$), the uncertainties in tracer calibration (0.03%; Condon et al., 2015; McLean et al., 2015) and U decay constants (0.108%; Jaffey et al., 1971) should be added to the internal error in quadrature. Quoted errors for calculated weighted means are thus of the form ±X(Y)[Z], where X is solely analytical uncertainty, Y is the combined analytical and tracer uncertainty, and Z is the combined analytical, tracer and $^{238}U$ decay constant uncertainty. The CA-ID-TIMS method was performed at the Department of Geosciences, Boise State University, Idaho, USA.

### 3.2. Palynology

A set of 19 samples was selected for palynological and palynofacies analysis. Approximately 10 g of sediment was crushed and treated with 10% HCl to remove carbonates, followed by 47% HF at 55 °C to remove silicate minerals following the protocol of Wood et al. (1996). Residues were washed with deionized water until a neutral pH was reached, and then sieved at 10 μm. The palynological preparation was carried out at the School of Materials and Chemistry & Chemical Engineering, Chengdu University of Technology. The samples were further macerated at the Laboratory of the Croatian Geological Survey. Heavy liquid separation with $ZnCl_2$ (specific gravity 2.1 kg/l) was performed on each sample in order to concentrate the organic residue and separate it from the remaining mineral particles. Slides were embedded in glycerol, and additional slides were mounted in silicon oil. Microscope analysis was carried out with an Olympus BH2 RFC trinocular transmitted light microscope equipped with a fluorescence light source at magnifications of ×100, ×200 and ×400. Photomicrographs were taken with an AmScopeTM camera adapter connected to AmScope v.3.7 camera software. For palynofacies analysis, 300 organic particles were counted. The terminology of dispersed organic matter was adopted from Jaramillo and Oboh-Ikuenobe (1999) and Mendonça Filho et al. (2012).

### 3.3. Organic carbon isotopic analysis

A total of 137 samples were collected through the Chang 7 Member and the lower part of Chang 6 Member of core Z40 for $\delta^{13}C_{org}$ analysis. Of these, 29 samples are shaly siltstones, 5 are oil-contaminated shales, 23 are sandstones, 60 are shales and 20 are siltstones. Bulk rock samples were washed with deionized water to clean the superficial dust. The dried rocks were then powdered in an agate mortar. Around 2 g of powdered sample were treated with 50 ml of 10% HCl for 24 h. The residuals were cleaned with deionized water and centrifuged until the pH of the solution was ca. 7. The residuals were then dried at 55 °C.

Approximately 1–2 mg of sample were weighed in tin capsules. The $\delta^{13}C_{org}$ analyses were conducted at the Department of Geosciences, University of Padova, Italy, using a Thermo Flash 2000 Elemental

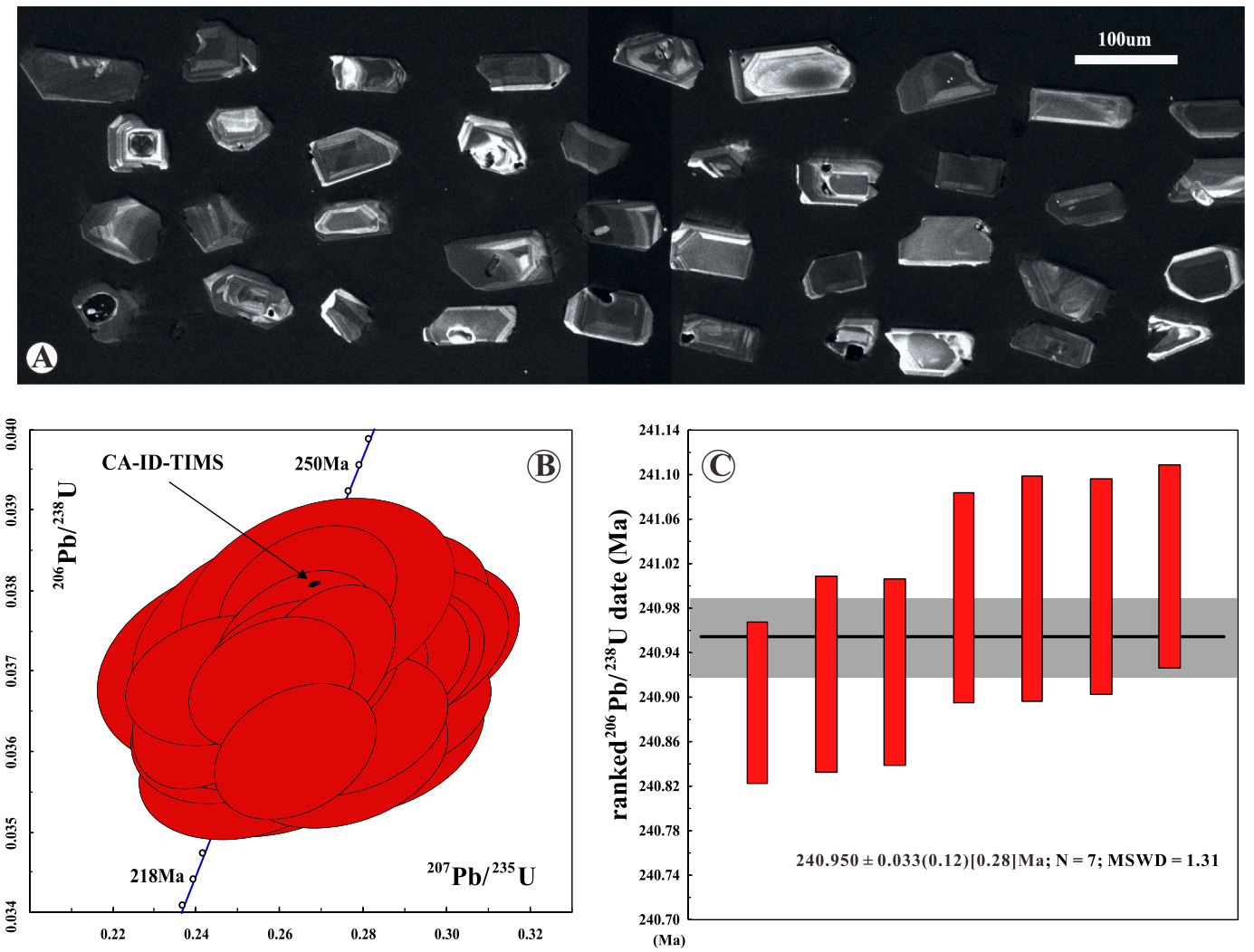


**Fig. 3.** A). Representative cathodoluminescence (CL) images of volcanic zircons from tuff sample Z40–2. B—C). Results of CA-ID-TIMS dating of sample Z40–2. The weighted mean $^{206}Pb/^{238}U$ age is 240.950 ± 0.033 (0.12) [0.28] Ma (2σ).

Analyzer linked to a Thermo Delta V advantage isotopic ratio mass spectrometer. Results were normalized to the standard δ notation relative to VPDB by analyzing contemporaneously two international standards of IAEA CH-7 (−32.151‰) and CH-6 (−10.449‰). A quality control standard was also run along with the samples (ZER, a sucrose from a C3 plant). The analytical precision was better than ±0.15‰ (1σ) during the period of the analyses.

## 4. Results

### 4.1. TIMS zircon U/Pb ages

CL imaging of zircon crystals revealed a consistent population of moderately to brightly luminescent, oscillatory-zoned crystals (Fig. 3A). A small number of crystals have irregularly shaped, relatively non-luminescent cores overgrown by the aforementioned luminescent, oscillatory rims. Seven grains were selected for CA-TIMS analysis on the basis of the uniform, predominant CL pattern, avoiding those crystals with resorbed non-luminescent cores, and consistent in-situ U—Pb dates. All seven analyses are concordant and equivalent (Fig. 3B), with a weighted mean $^{206}Pb/^{238}U$ date of 240.950 ± 0.033 (0.12) [0.28] Ma (Fig. 3C, MSWD = 1.31), which is interpreted as dating the eruption and deposition of this ash bed.

### 4.2. Organic carbon isotopes

The $\delta^{13}C_{org}$ values in core Z40 range between −31 and − 25‰ (Figs. 2, 4). $\delta^{13}C_{org}$ values of 29 shaly siltstones, 5 oil contaminated shales, 23 sandstones, 60 shales, 20 siltstones range from −29.5 to −25.6‰, −31.3 to −29.0‰, −29.7 to −25.8‰, −31.2 to −25.8‰, −28.7 to −26.0‰, respectively. The range of $\delta^{13}C_{org}$ values of coarser sediments, i.e., sandstones and siltstones, are close, somehow heavier than those of shales (Fig. 4). The oil-contaminated shales have the most negative $\delta^{13}C_{org}$ values (Figs. 2, 4).

The $\delta^{13}C_{org}$ values of shales present a distinct positive upward trend from 1480 m to 1450 m, then maintain stable $\delta^{13}C_{org}$ values within 1450 m to 1428 m. A pronounced excursion defined by an abrupt −3.5‰ negative shift in $\delta^{13}C_{org}$ (CIE 1) is centered at ca. 1423 m. After the CIE 1, $\delta^{13}C_{org}$ values increase gradually, reaching −26‰ at 1412 m, followed by a ca. −4‰ negative carbonisotope excursion (CIE 2) at ca. 1405 m. A third negative shift (CIE 3) of −4.2‰ is seen just above the CIE 2 and centered at 1370 m (Fig. 2).

### 4.3. Palynofacies and palynomorphs (spores and pollen)

The palynofacies analysis revealed that the particulate sedimentary organic matter is exclusively of terrestrial origin. Overall, the phytoclast group is predominant; and palynomorphs, including spores and pollen, are only minor components (<10%) (Fig. 5, for raw data see Supplementary dataset). Phytoclasts are fragments of tissues derived from terrestrial plants (Mendonça Filho et al., 2011, 2012). The majority of these phytoclast particles are black to brown, non-biostructured or with a highly degraded biostructure, often with “pseudoamorphous” or gelified appearance, and with diffuse edges under transmitted white light (Fig. 5). These particles are often degraded and reworked to a point where they closely resemble amorphous products from phytoplankton or bacteria (Tyson, 1995; Silva et al., 2014). Their angular to sub-angular outlines suggest that they are likely derived from plant fragments. They can also appear as aggregates with small-sized phytoclast inclusions, but they rarely mask palynomorphs. The degraded morphological features and weak or lack of fluorescence (Fig. 5J) is related to microbial degradation and reworking (Oboh-Ikuenobe et al., 1998; Mendonça Filho et al., 2011; Ţabără et al., 2015; Zhang et al., 2015). They represent the minimum of 32% of the particles, and often contribute to nearly 100% of the sedimentary organic matter, especially in the Chang $7_3$ submember (Fig. 2).

The abundance of non-opaque biostructured wood particles (banded and pitted) (Fig. 5) ranges between 3% and 55% of the total organic particles with an average of 19%. Their proportion only increases somewhat in submembers Chang $7_2$ and Chang $7_1$ and in the lower part of Chang 6 from 1424 m upwards, but the values are quite variable (Fig. 2). Non-structured, pale yellow-green, sheet-like membranes and opaque charcoal particles are subordinate (<20%). Palynomorphs are very rare with higher counts confined to the samples at 1424 m, 1402.8 m, 1388 m, 1374.6 m, and 1361.1 m.

The palynomorph spectrum is dominated by bisaccate non-striate

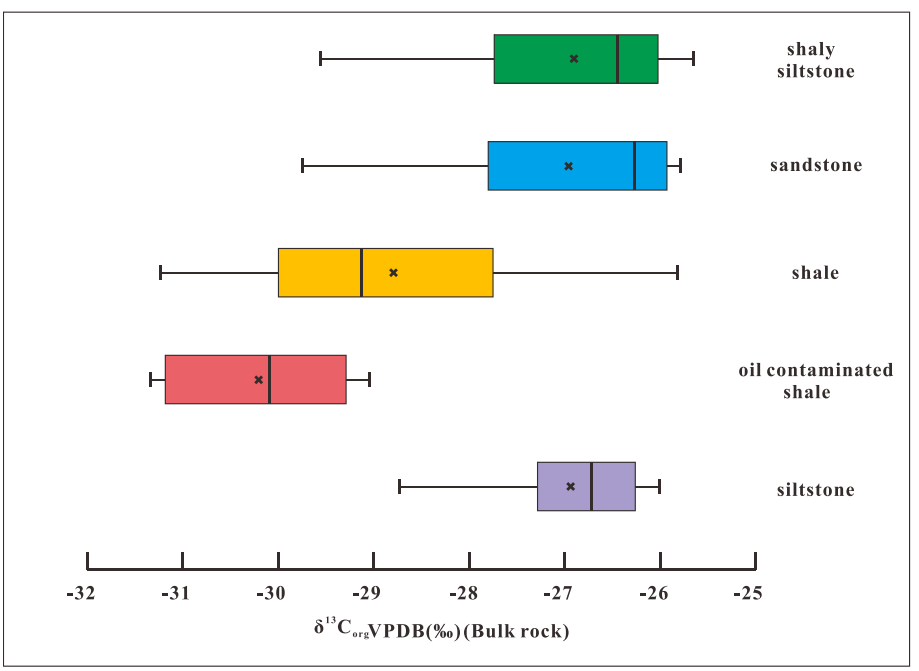


**Fig. 4.** Box plots of $\delta^{13}C_{org}$ values of bulk rocks of the core Z40. The boxes represent 25% and 75% quartiles, the whiskers depict 10% and 90% ranges, the black central crosses in the box depict the averages, and the central lines in the box depict the medians.

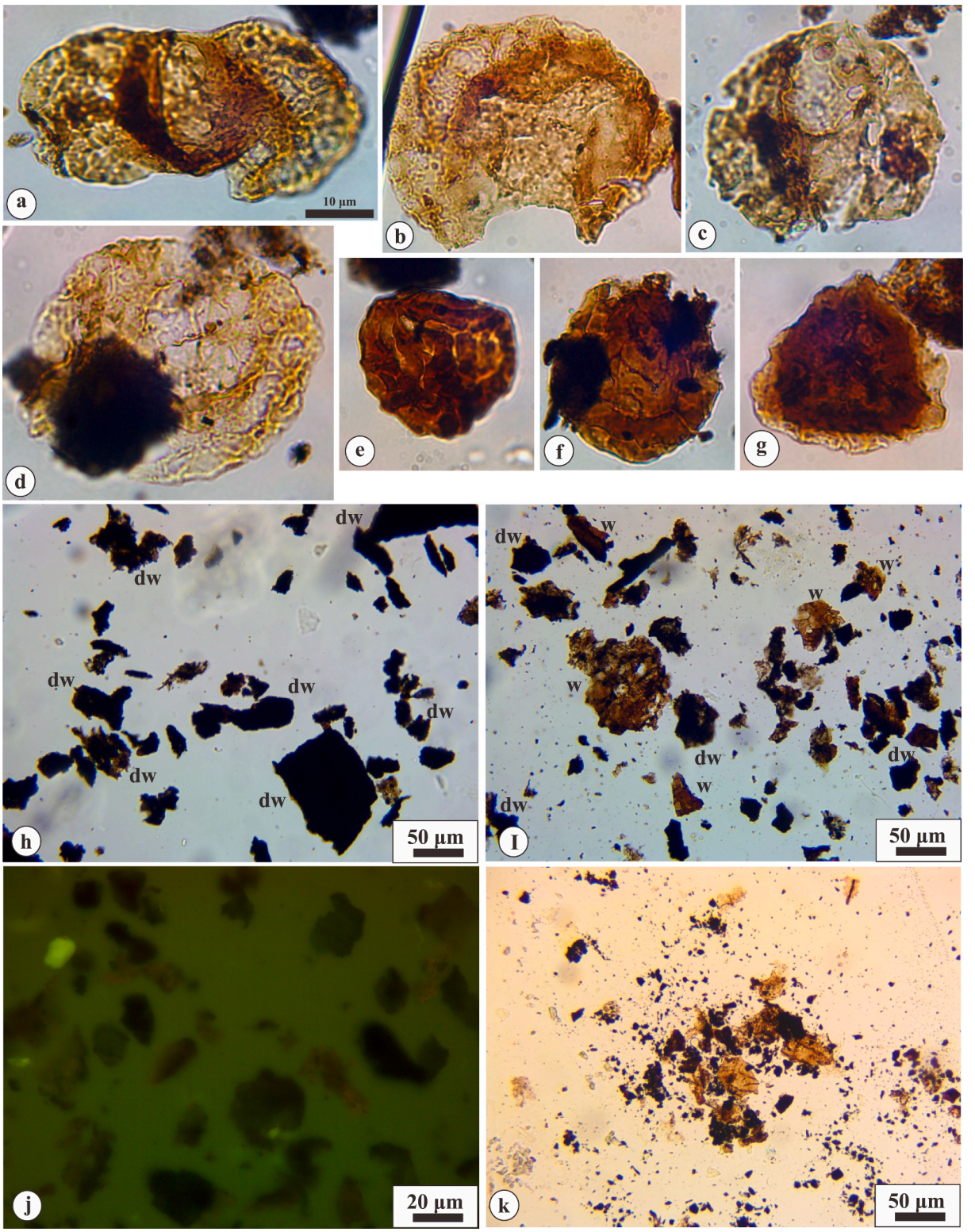


**Fig. 5.** Selected palynomorphs (a-g) and palynofacies (h-k) from the core Z40. Scale bar of 10 µm shown as bar (a) applies to each palynomorph image in (a-g). (a) *Platysaccus queenslandi*, 1380.6 m level. (b) *Florinites?* sp. 1361.1 m. C) *Chordasporites* sp. 1455 m. (c) *Parataeniaesporites striatus* 1410.2 m. (e-f) *Asseretospora* sp. 1380.6 m. (g) *Kreauselisporites guangyuensis* 1374.6 m. (h) Palynofacies at 1474.4 m with a predominance of degraded "pseudoamorphous" black-brown wood particles (dw). (i) Palynofacies at 1420.3 m with predominantly degraded "pseudomorphs" wood (dw) and biostructured phytoclasts (w). Despite the lack of distinct structure and "fuzzy" edges, the angular-tabular appearance of these particles indicate a terrestrial origin. (j) Palynofacies at 1420.3 m in fluorescence light. Note the total lack or very weak fluorescence of the organic particles. (k) Palynofacies at 1361.1 m. Note the increase of more transparent plant debris, but the degraded particles with pseudoamorphous appearance are still predominant. (For interpretation of the references to colour in this figure legend, the reader is referred to the web version of this article.)

and striate pollen grains. Non-saccate pollen grains and spores are scarce, usually 1–5 grains. Overall, the preservation of the palynomorphs is poor due to diagenetic pyrite overgrowths, and the majority of them can be identified only on generic level. The identification of palynomorphs (and all particles) is further challenged by the relatively high thermal maturity of the kerogen in the Chang 7 shales that indicate 429–476 °C heating due to burial (Zhang et al., 2015). Most of the samples are rich in phytoclasts, thus the palynomorphs are extremely diluted by the plant debris. The highest palynomorph abundances are recorded in the samples from the upper part of Chang 7 and Chang 6. The maximum abundance and diversity are attained in the sample at 1380.6 m with 17 identified taxa (see Supplementary dataset). Selected palynomorphs are illustrated in Fig. 5 and Fig. SF2, SF3, SF4. Spores are represented by various fern spores: *Asseretospora* (Fig. 5E-F), *Verrucosisporites*, *Deltoidospora*, *Triquitrites,* and *Osmundacidites*. The most common taxon is the fern spore, *Asseretospora* sp. Lycopsid spores, e.g., *Aratrisporites*, *Lycopodiumsporites clavatoides*, and *Kraeuselisporites* spp. (Fig. 5G) are less frequently recorded. Mosses are subordinate and are represented only by *Annulispora*. Non-striate bisaccate pollen grains, *Alisporites australis, A. parvus, Klausipollenites decipiens,* and *Protopicea* are more common. Striate bisaccate pollen grains *Parataeniaesporites* (Fig. 5D) and *Chordasporites* (Fig. 5C), occur only as minor constituents. Cycad pollen (*Cycadopites*) is continuously recorded, but only 1–2 grains occur in the samples.

## 5. Discussion

### 5.1. Age of Chang 7 Member in core Zheng 40, southern Ordos Basin

#### 5.1.1. Age span implied by radioisotopic dates

Tuff interlayers in the lowermost portion of the Chang 7 Member (Chang $7_3$ submember) of the Yanchang Formation have been reported across the entire Ordos Basin and served as key beds for stratigraphic subdivision and correlation. They have been dated by different U—Pb methods and have yielded a wide age range of ca. 241.6 Ma to 226.5 Ma, which spans Middle Triassic to Late Triassic (Fig. 6; Deng et al., 2013; Wang et al., 2014; Zhang et al., 2014; Wang et al., 2017b; Zhu et al., 2019; Sun et al., 2020 and this study). Sun et al. (2020) argued that this variability may be partly due to the fact that tuffs at the base of Chang 7 were not always the same. Sun et al. (2020) explained this by discussing that two depocenters existed in the Ordos Basin, and therefore the stratigraphic record (including tuff layers) of the two subbasins may be diachronous, hence different tuffs may have been sampled in different sections/boreholes.

However, concordant U—Pb dates of ca. 241 Ma to 239 Ma are obtained in the same lower Chang 7 Member from the northwestern (core Luo 36), western (core Zhuang 211) and southern (Yaoqu section) parts of the Ordos Basin (Fig. 1C). Our U—Pb date (240.950 ± 0.033 Ma) that was obtained by applying the CA-ID-TIMS method to zircons from the middle portion of the Chang 7 Member (Chang $7_2$ submember) in core Z40 indicates an early Ladinian age. This implies that the underlying Chang $7_3$ submember in core Z40 cannot have a younger Carnian age, as implied by the reported date from a tuff layer in Chang $7_3$ submember from the Yunmeng section (Sun et al., 2020).

One reason for the apparent discrepancy in ages is that applying different techniques of zircon chronology may yield quite different U—Pb dates from the same sample. In this paper, an initial age was derived from the ablation of zircons were the LA-ICP-MS method. The resulting date of 233.5 ± 1.0 Ma is ca. 7 Myr younger than our more precise date of 240.95 ± 0.033 Ma obtained by the applying the CA-ID-TIMS method (Fig. 6 and Fig. SF1, also see in Supplementary dataset). Indeed, there is no overlap in the reported laboratory uncertainties in the dates from those two different methods. The more accurate CA-ID-TIMS method eliminates laser-induced matrix effects, mitigates and evaluates Pb loss, and resolves complexities of interpreting lower-precision, normally-distributed LA-ICP-MS dates. Therefore, our study which applied both techniques highlights the need for obtaining high-precision CA-ID-TIMS dates for timescale applications, and that the LA-ICP-MS method can result in misleading age estimates. Therefore, we only focus on TIMS-derived dates in our discussion.

The new age determination allows correcting the sediment accumulations rates that had been previously estimated for the Chang 7 Member. The cyclostratigraphy of the Chang 7 Member reported by Chen et al. (2019) and Zhang et al. (2019b) revealed apparent (shale decompaction has not been calculated) sediment accumulations rates ranging from 0.9 cm/kyr to 2.1 cm/kyr. In contrast, our new zircon dating yields an apparent average sediment accumulations of 9.7 cm/kyr for the Chang $7_3$ submember and the lower part of Chang$7_2$ submember. This significantly higher value is a remarkable sedimentation rate for an intracratonic basin and requires reexamination of the assumptions used in assigning the astronomical cycles in the previous cyclostratigraphy analyses.

#### 5.1.2. Age span implied by palynology assemblages

Deng et al. (2018), on the basis of plants, palynomorphs, vertebrate fauna, ostracods and bivalves combined with high-resolution

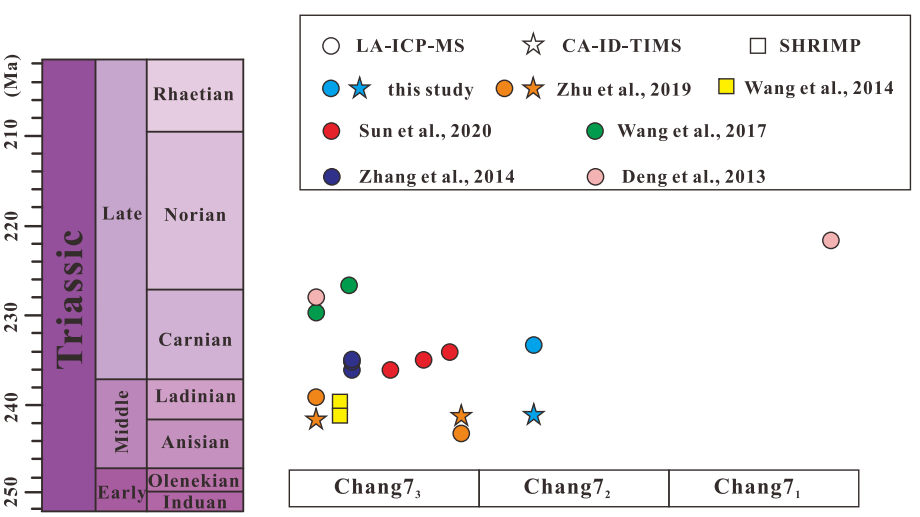


**Fig. 6.** Published U/Pb dates obtained by applying different dating methods to the Chang 7 Member in the Ordos Basin. Note: the zircon age positions are relative, and the U/Pb ages obtained from the SHRIMP and TIMS methods are generally older than those obtained from LA-ICP-MS method in the same sampling level. The Triassic chronostratigraphic timescale follows Ogg et al. (2020).

radioisotopic dating from the Yanchang Formation, suggested that the age span of Chang 10 through Chang 7 members should be late Anisian to Ladinian. The palynological assemblage that we identified in core Z40 corresponds to the *Asseretospora-Apiculatisporites-Chordasporites* assemblage (AAC) (Fig. 2) according to the subdivision of Deng et al. (2018), to the *Asseretospora-Walchiites* (AW) assemblage according to the scheme of Ji and Meng (2006) from the eastern Gansu province (SW Ordos Basin), and to the *Duplexisporites-Chordasporites* subzone of Zhang et al. (1982) from the southern Ordos Basin. The recorded assemblage is also similar to the *Duplexisporites-Parataeniaesporites* assemblage of Shang (1998) from the Shaanxi-Gansu-Ningxia Basin. In the Ordos Basin, the boundary between the AAC and the underlying older *Punctatosporites-Aratrisporites-Verrucosisporites* palynological assemblage is at the base of the Chang 7 (Deng et al., 2018). By contrast, both Liu et al. (1981) and Qu et al. (1983) placed assemblage boundaries between the Chang 7 and Chang 6 members. In other sections, spores from the AAC assemblage are composed mainly of zonate forms e.g., *Asseretospora* (synonyms *Duplexisporites, Striatella)*, *Kaeuselisporites*, *Kyrtomisporis*, *Annulispora*, *Limatulasporites*, *Polycingulatisporites*, *Densosporites*, *Triquitriletes* (Deng et al., 2018). The pollen grains are dominated by non-striate bisaccate pollen and monocolpate pollen (*Cyacadopites*) (Deng et al., 2018). Bisaccate pollen grains with single striation are less numerous e.g., *Parataeniaesporites*, or *Chordasporites* (Deng et al., 2018). Monosaccate pollen e.g., *Cordaitina*, *Florinites*, and *Accinctisporites* are scarce (Deng et al., 2018).

Previous palynological analysis suggested a Late Triassic (Carnian) age for the AAC and AW assemblages (Qu, 1980; Ji and Meng, 2006; Deng et al., 2018). However, many spore and pollen taxa from Chang 7 and Chang 6 of the Yanchang Formation are long-ranging species transitioning through the Middle and Late Triassic. *Asseretospora scanicus* is present from Carnian strata in the Xuijahe Formation in the Sichuan Basin (Li et al., 2016). From the Tarim Basin in the NW China, Peng et al. (2018) interpreted the age of a palynological assemblage with abundant spiny trilete spores (*Apiculatisporites*, *Anapiculatisporites*, *Acanthotriletes*), low abundance of *Dictyophyllidites harrisii, Concavisporites toralis*, and without *Lunatisporites* spp. and *Limatulasporites* spp. as late Middle Triassic. In that Tarim Basin, *Striatella* spp. (synonym *Asseretospora*) occur in much lower numbers in the Carnian-Norian palynological assemblages compared to higher abundance values in the late Middle Triassic (Peng et al., 2018). Therefore, due to the high frequency of *Asseretospora* in the investigated section, it is possible that the studied interval of Chang 7 is still Ladinian.

The correlation of the palynoflora beyond the Ordos Basin is complicated by the lack of the characteristic Middle and Late Triassic marker species to compare to the Tethyan and Germanic realms (e.g., Roghi, 2004; Kürschner and Herngreen, 2010; Mietto et al., 2012). The characteristic Circumpolles taxa (*Praecirculina, Partitisporites, Duplicisporites, Camerosporites*), and monosaccate pollen (*Patinasporites densus, Vallasporites ignacii, Enzonalasporites vigens*, *Pseudoenzonalasporites summus*) were not reported from Chang 7 or Chang 6 by previous palynological studies. *Echinitosporites iliacoides*, which is characteristic of the Ladinian in the Boreal realm (Paterson and Mangerud, 2019), has not been documented from the Yanchang Formation. Similarly, Australian (Gondwana) marker species for the late Middle Triassic-early Late Triassic, e.g., *Staurosaccites quadrifidus* (Helby et al., 1987), are absent.

The Ordos Basin was located within the North China palynofloral province during the Triassic which spread north to the Palaeo-Qinling, Palaeo-Qilianshan and Palaeo-Tianshan mountains (Qu et al., 1983; Shang, 1998). This province is primarily characterized by cosmopolitan taxa (Qu et al., 1983; Peng et al., 2018). According to Shang (1998) the palynofloral composition of the province is most similar to that of Siberia and Kazakhstan (Rovnina, 1973; Sakulina, 1973). In the Cis-Uralian region and Siberia, the systematic occurrence of *Duplexisporites* (=*Asseretospora*) and *Florinites* species is considered to be characteristic of the Middle Triassic (Ilyina and Egorov, 2008; Tverdokhlebov et al., 2020) suggesting a similar age for the Chang 7 Member in the Ordos Basin.

The macroflora of the Chang 7 Member suggests a late Middle Triassic age (Deng et al., 2018). The boundary between the *Sympteris-Danaeopsis magnifolia* and the succeeding *Thinnfeldia-Danaeopsis fecunda* assemblages coincides with the Chang 7 and Chang 6 boundary (Deng et al., 2018). The older assemblage is assigned to the late Middle Triassic based on the presence of *Annalepis* in Chang 8 and the lower part of Chang 7 (Deng et al., 2018). The younger *Thinnfeldia-Danaeopsis fecunda* flora is comparable to European Keuper vegetation of Carnian-early Rhaetian age (Deng et al., 2018). In addition, *Danaeopsis fecunda*, characteristic of Chang 6, is confined to the Late Triassic in Europe (Kustatscher et al., 2012b). Other fossils, including bivalves, conchostracans, ostracods and fish, also support a late Middle Triassic age for Chang 7 (Liu, 1962; Su et al., 1980; Liu and Li, 1980; Wang and Liu, 1980). In summary, we conclude that Chang 7 Member of the Yanchang Formation in core Z40 is Ladinian, at least in part.

### 5.2. Ladinian vegetation and paleoclimate in the Ordos Basin

As the core Z40 yielded relatively few and moderately to poorly preserved taxa; therefore, the vegetation and paleoclimate interpretation is based on integrating the present dataset with previously published palynological and paleobotanical records. Overall, the sporomorphs preserved in the distal lake setting of the Chang 7 Member from Z40 likely reflect the vegetation of the surrounding catchment areas. The large size of the lake system implies that pollen came from a large area (Jacobson and Bradshaw, 1981).

The most abundant palynomorph group in Z40 are bisaccate pollen grains, which could have been produced by Corystospermalean seed ferns or conifers. These conifers can be considered as extrabasinal hinterland elements that represent drier areas further from the lake system (Kustatscher et al., 2010, 2012a). Since these pollen grains are highly buoyant, they can be transported by wind over large distances before they enter the lacustrine basin (Tyson, 1995). Lowlands were characterized by an open canopy of seed ferns with the understory of ferns and lycopsids (e.g., Lindström et al., 2017). The most abundant spore taxon in Z40, *Asseretospora* sp., and the less common *Kraeuselisporites* group are assigned to the coastal vegetation group (coastal SEG) in the Sporomorph Ecogroup model (SEGs) of Abbink (1998), see Kustatscher et al., 2012a); but here in the Ordos Basin, these spores probably indicate plants colonizing wetter environments on the lake shores and in mires. The spores *Osmundacidites*, *Apiculatisporites*, *Lycopodiumsporites*, and *Uvaesporites* indicate wet lowland or riverbank-deltaic communities according to the SEG model (Abbink, 1998; Kustatscher et al., 2012a; Paterson et al., 2017).

The overall dominance of hygrophytic plant groups (e.g. lycopsid and fern spores) together with the local macrofossil data from Chang 7 and Chang 6 indicates a prevailing humid environment and a warm, wet, subtropical-temperate climate (Shang, 1998; Ji and Meng, 2006; Ji and Zhu, 2013). Widespread warming during the early Ladinian has been attributed to the intensification of the Pangaea-Tethys monsoonal circulation (Trotter et al., 2015; Chu et al., 2020).

### 5.3. $\delta^{13}C_{org}$ record from the late-Middle Triassic in the Ordos Basin

The variations of $\delta^{13}C_{org}$ values from the Chang $7_3$ to Chang $7_1$ submembers in the core Z40 (Fig. 2) seem to be facies related and influenced by the mixing of organic matter from different sources. In the $\delta^{13}C_{org}$ record from core Z40, isotope values of coarser-grained sediments of siltstones and sandstones are less negative than those of finer sediments (shales) (Fig. 4). From 1424 m upwards in Z40, a shift to coarser and more varied lithologies and to oscillations in $\delta^{13}C_{org}$ values coincides with increased fluctuation in the abundance of structured wood and degraded pseudoamorphous organic particles (Fig. 2). This attests that, in general, coarser sediments of sandstone and siltstone are more likely to incorporate more terrestrial organic matter. In contrast,

the organic matter preserved within finer clay-rich sediments deposited in the oxygen-depleted, low-energy and deeper water conditions in the Chang $7_3$ submember probably has a larger contribution from lacustrine biomass or microbial degradation with more negative carbon isotope ratios (e.g., Meyers, 1994; Andrusevich et al., 1998).

However, the sources of organic matter in the Chang 7 shales may be a mixture of terrestrial and aquatic (algal, bacterial) biomass. The sapropel kerogens (Type I kerogen) are most common in the lower part of the Chang $7_3$ submember (Ji et al., 2007; Lin et al., 2013; Zhang et al., 2015; Li et al., 2020), whereas the shales in the Chang $7_2$ and Chang $7_1$ submembers mainly contain thermally mature Type II and III kerogen (e.g., Li et al., 2020). Type I kerogen of lacustrine origin is principally derived from planktonic green algae (Talbot, 1988) and is characterized by low $\delta^{13}C_{org}$ values, generally ranging from −30 to −25‰ (Meyers, 1994). Ji et al. (2007) reported $\delta^{13}C_{org}$ values of kerogen in the Chang $7_3$ shales ranging from ca. −30 to −28‰, which are close to the $\delta^{13}C_{org}$ values of Chang $7_3$ shales in core Z40 (Fig. 2). Conversely, Type II and III kerogens are mainly derived from terrestrial plant organic matter, and usually have higher $\delta^{13}C$ values near −25‰ (Andrusevich et al., 1998; Ji et al., 2007).

Sandy levels can be expected to be more prone to later contamination by hydrocarbons migrating in the sediment because of their higher permeability. By contrast, the low-permeability shales may have preserved a more pristine isotope composition of the organic carbon. Therefore, we decided to exclude sand-rich intervals and to interpret the only the features recorded in the $\delta^{13}C_{org}$ from the shale record in core Z40. An upward positive trend in $\delta^{13}C_{org}$ values is recorded in the Chang $7_3$ submember of core Z40 (Fig. 2), and then $\delta^{13}C_{org}$ values remain close to −26‰. This positive trend is a well-known feature of the Middle Triassic stable isotope record, and has been repeatedly observed both in marine carbonates (e.g., Korte et al., 2005; Preto et al., 2009) and terrestrial organic matter (e.g., Dal Corso et al., 2011). Three negative carbon isotopic shifts (CIE 1 to CIE 3) can be recognized in the shales of the Chang $7_2$ and Chang $7_1$ submembers (Fig. 2). Unfortunately, there are only few high-resolution records of $\delta^{13}C_{org}$ values throughout Chang 7 Member, or for the Ladinian in general; therefore, the significance of these CIE features is uncertain. Records of $\delta^{13}C_{carb}$ from marine carbonates do not display similar sharp negative excursions within the Ladinian. Therefore, as a preliminary hypothesis, we suggest that the sharp CIEs in the Ladinian of core Z40 may be related to changes in the kerogen types due to different organic matter sources (e.g., Li et al., 2020), rather than excursions in the global carbon cycle.

### 5.4. *A possible causal link between lake expansion and sea-level change during the early Ladinian?*

The southern Ordos Basin has been interpreted as an intracontinental foreland basin that developed as a consequence of the collision between North China and South China blocks. The deposition of the Yanchang Formation also coincided with the closure of the Paleotethys in southwestern China (Liu and Yang, 2000; Yan et al., 2019). That collision between Cathaysia and drifting Cimmerian plates led to the Indosinian orogeny (Golonka, 2007), and may have been responsible for global sea-level fluctuations (Hornung et al., 2007). There is circumstantial compelling evidence from the heavy sulfur isotopic composition of pyrite (Wang et al., 2017a; Chen et al., 2020) and high Sr/Ba ratios (Li et al., 2020) that a marine connection persisted during the deposition of the Chang 7 Member. Liu et al. (1999) proposed that the early-middle Mesozoic water masses from the Tethys ocean entered the Ordos Basin through a passage in the present Liupanshan Mountain or a southern area (southwest Ordos Basin). Hence, the question arises whether the lake expansions and fluctuations in depth were influenced by eustatic sea-level variations.

Different hierarchies of transgressive/regressive cycles have been identified in the Yanchang Formation. The highest-rank transgressive cycle began in the Middle Triassic with the initiation of lacustrine sedimentation, and culminated with a phase of lake deepening as interpreted from the deposition of laminated black shales and gravity flow sediments (related to deep-lake fan system) within the Chang 7 and Chang 6 members (e.g., Liu et al., 2015; Guo et al., 2018). The maximum deepening of the lacustrine system has been placed in the mid-lower portion of Chang 7 Member (Chang $7_3$ submember) that is dominated by black shales (e.g., Zou et al., 2010; Yang and Deng, 2013). The deepest-water conditions in most of the Ordos Basin occur at the base of the Chang $7_3$ submember as indicated by the thickest interval of black shales, such as those seen in core Z40. Black shales are still abundant in the overlying Chang $7_2$ submember, but gradually decrease in frequency (Fig. 2).

Our high-resolution radioisotopic date from the lower middle portion of the Chang $7_2$ submember, when combined with biostratigraphic data and available radioisotopic dates from the base of the Chang $7_3$ submember, allow bracketing of the phase of maximum lake expansion as between 240.95 ± 0.033 Ma (this paper) and 241.56 ± 0.09 Ma (Zhu et al., 2019) during the earliest Ladinian. The earliest Ladinian interval was also the culmination of the transgressive part of a 3rd order T/R cycle that is documented in marine settings of the Western Tethys realm (Fig. 7). In the Central European Basin and in Iberia, the shallow-sea limestones of the Upper Muschelkalk unconformably onlap alluvial to marginal marine beds (Gianolla and Jacquin, 1998; Escudero-Mozo et al., 2015; Franz et al., 2015). A rapid transgression during the late Anisian in the Central European intracratonic basin culminated in the emplacement of a large semi-enclosed inland sea (Franz et al., 2015). In the Southern Alps, the maximum flooding surface of a major 3rd order cycle (e.g., Gianolla et al., 1998) falls within the *Chieseiceras chiesense* ammonoid subzone (uppermost *Nevadites* Zone, cf. Mietto and Manfrin, 1995; Balini et al., 2010), which is dated to about 241.5 Ma (uppermost *Secedensis* Zone in Brack et al., 2005; Wotzlaw et al., 2018). This maximum flooding surface is recognized at the supraregional level and was thus interpreted as an early Ladinian maximum of eustatic sea-level (Hardenbol et al., 1998; Haq, 2018; Fig. 7). High-precision radioisotopic dates from the maximum flooding interval in the Dolomites (Wotzlaw et al., 2018) are very close to those retrieved from Chang 7 of the Yanchang Formation.

One option to explain the Ladinian deepening of the Ordos lake system is to related it to an episode of intensified orogenic activity in the nearby Qinling belt, which may have caused far-field effects of increased rates of subsidence in the Ordos Basin (e.g., Liu et al., 2013; Yang and Deng, 2013; Gao et al., 2020). An imbalance between the distribution of sediment supply and that increased rate of subsidence may have induced deepening of portions of the lake. Multiple episodes of synsedimentary tectonic activity have been documented during the deposition of the Chang 7 member, and have been suggested to control the evolution of the southwest Ordos Basin (e.g., Gao et al., 2020). However, the initial stage of this regional tectonic movement has been proposed to occur from 238 Ma to 230 Ma (Deng et al., 2013), therefore during the following Carnian. Based on evidences from sedimentology and zircon U—Pb ages, Zhang et al. (2019a) also stressed that the onset of the influence of regional tectonic activity was at ca. 233 Ma within the Ordos Basin. This regional tectonic activity, which has been interpreted as occurring during the Carnian, is younger than the Ladinian depositional age of the Chang $7_3$ submember. In addition, a general deepening and expansion of a large lake requires an increase in its water volume, although an increased subsidence rate might cause local depressions with increased water depths within its basin if the rest of the lake system became shallower or more restricted. Instead, we suggest that global eustasy, coupled with a restricted partial connection of the Ordos lake system to the nearby seaways contributed to the deepening of the Ordos lake.

We propose that the maximum deepening of the lacustrine system of the Ordos Basin coincided with, and was probably influenced by, the early Ladinian maximum in eustatic sea-level. A similar situation, in which eustatic oscillations influenced the level of vast lake systems, has

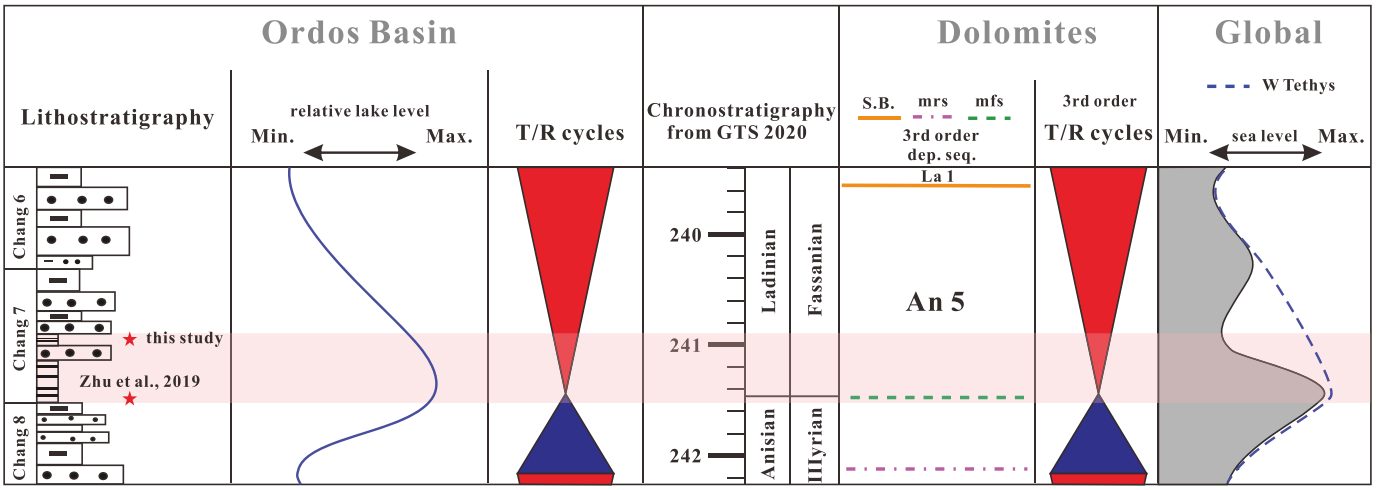


**Fig. 7.** Late Anisian to early Ladinian lake-level variations in the Ordos Basin compared to sea-level oscillations observed in the geo-chronologically calibrated sedimentary records from the Dolomites in the Western Tethys and to the interpreted global eustatic signal. T/R = transgressive/regressive cycles; S.B. = sequence boundary; m.r.s. = maximum regressive surface; m.f.s. = maximum flooding surface. The lithostratigraphy and lake-level fluctuations of Yanchang Formation modified from Yang et al. (2017). The sequence stratigraphy of the Dolomites follows Gianolla et al. (2021). The global sea-level variations follow Haq (2018). The chronostratigraphy from GTS 2020 follows Ogg et al. (2020).

been described in the Toarcian (Early Jurassic) of the Sichuan Basin by Xu et al. (2017, 2021). However, despite the marine connection and influence as interpreted from the geochemical data, the salinity of the main Ordos Basin lake system remained largely freshwater (e.g., Ji et al., 2006; Bai and Ma, 2020). Marine incursions, when these happened, were likely primarily intruding only into the deeper stratified parts of the lake due to density differences (e.g. Xu et al., 2021). The generally warm climate and intensification of the Pangaea-Tethys monsoon provided the abundant freshwater supply to the surface waters that amplified and maintained the lake expansion (Chu et al., 2020; Xu et al., 2021).

## 6. Conclusions

This study presents a high-precision U—Pb date (TIMS method) from zircons, palynofacies analysis and high-resolution $\delta^{13}C_{org}$ record were obtained from core Zheng 40 through the Chang 7 Member of the Yanchang Formation in the Ordos Basin (China). The radioisotopic date from the middle portion of Chang 7 Member yields 240.950 ± 0.033 Ma and the identified palynological assemblage, which is correlated to the *Asseretospora-Apiculatisporites-Chordasporites* assemblage (AAC), indicate that Chang 7 deposited during the Ladinian. The $\delta^{13}C_{org}$ record with three main negative excursions derived from shales in core Zheng 40 is considered more reliable than isotope values from sandy samples. Although the causes of these negative shifts in $\delta^{13}C_{org}$ are still unclear, these may provide means for correlation of Ladinian strata within the Ordos Basin and, potentially, between continental and marine successions. The enhanced chronostratigraphic framework of the Chang 7 Member assigns the phase of maximum expansion of the Ordos Basin lacustrine system to the earliest Ladinian. Marine incursions into the deeper stratified depths of the Ordos lake system has been suggested by geochemical proxies. The comparison with coeval well-dated eustatic sea-level oscillations recorded in the Western Tethys suggests that lake-level in the Ordos Basin might be, at least in part, controlled by eustasy; and that the earliest Ladinian sea-level highstand contributed to the timing of such a marine incursion into the Chang 7 Member of the Yanchang Formation.

## Declaration of Competing Interest

The authors declare that they have no known competing financial interests or personal relationships that could have appeared to influence the work reported in this paper.

## Acknowledgements

We acknowledge Qiangwang Wu for his assistance in core sampling. Jacopo Dal Corso (China University of Geosciences) is thanked for valuable discussions. We are grateful to Editor Maoyan Zhu and two anonymous reviewers for their insightful suggestions that significantly improved the manuscript. Gabi Ogg prepared the graphic abstract. This work was supported by grants from the National Natural Science Foundation of China (grant numbers 41902106) and the State Key Laboratory of Loess and Quaternary Geology (grant number SKLLQGZR2005). The Triassic palynological studies of Viktória Baranyi are supported by the Croatian Geological Survey and a grant from the National Research, Development and Innovation Office of Hungary (NKFIH FK 134229 grant).

## Appendix A. Supplementary data

Supplementary data to this article can be found online at https://doi.org/10.1016/j.gloplacha.2021.103670.

## References

Abbink, O.A., 1998. Palynological identification in the Jurassic of the North Sea region. LPP (Laboratory of Palaeobotany and Palynology) Contrib. Ser. 8, 1–192.
Andrusevich, V.E., Engel, M.H., Zumberge, J.E., Brothers, L.A., 1998. Secular, episodic changes in stable carbon isotope composition of crude oils. Chem. Geol. 152, 59–72.
Bai, Y.L., Ma, Y.Y., 2020. Geology of the Chang 7 member oil shale of the Yanchang Formation of the Ordos Basin in central North China. Pet. Geosci. 26, 355–371.
Balini, M., Lucas, S.G., Jenks, J.F., Spielmann, J.A., 2010. Triassic ammonoid biostratigraphy: an overview. In: Lucas, S.G. (Ed.), The Triassic Timescale, 334. Geological Society, London, Special Publications, pp. 221–262.
Brack, P., Rieber, H., Nicora, A., Mundil, R., 2005. The Global Boundary Stratotype Section and Point (GSSP) of the Ladinian Stage (Middle Triassic) at Bagolino (Southern Alps, Northern Italy) and its implications for the Triassic time scale. Episodes 28, 233–244.
Catanzaro, E.J., Murphy, T.J., Shields, W.R., Garner, E.L., 1968. Absolute isotopic abundance of common, equal-atom, and radiogenic lead isotopic standards. J. Res. Natl. Bureau Stand. A 72A, 261–267.
Chen, G., Gang, W., Liu, Y., Wang, N., Guo, Y., Zhu, C., Cao, Q., 2019. High-resolution sediment accumulation rate determined by cyclostratigraphy and its impact on the organic matter abundance of the hydrocarbon source rock in the Yanchang Formation, Ordos Basin, China. Mar. Pet. Geol. 103, 1–11.
Chen, R., Liu, G., Shang, F., Cao, Y., 2020. Variations in hydrocarbon generating potential of the Chang 7 shale: evidence from pyrite morphology and sulfur isotope. J. Pet. Sci. Eng. 195, 107747.

Chu, R., Wu, H., Zhu, R., Fang, Q., Deng, S., Cui, J., Yang, T., Li, H., Cao, L., Zhang, S., 2020. Orbital forcing of Triassic megamonsoon activity documented in lacustrine sediments from Ordos Basin, China. Palaeogeogr. Palaeoclimatol. Palaeoecol. 541, 109542.
Condon, D.J., Schoene, B., McLean, N.M., Bowring, S.A., Parrish, R.R., 2015. Metrology and traceability of U–Pb isotope dilution geochronology (EARTHTIME Tracer Calibration Part I). Geochim. Cosmochim. Acta 164, 464–480.
Dal Corso, J., Preto, N., Kustatscher, E., Mietto, P., Roghi, G., Jenkyns, H.C., 2011. Carbon-isotope variability of Triassic amber, as compared with wood and leaves (Southern Alps, Italy). Palaeogeogr. Palaeoclimatol. Palaeoecol. 302, 187–193.
Darby, B.J., Ritts, B.D., 2002. Mesozoic contractional deformation in the middle of the Asian tectonic collage: the enigmatic Western Ordos fold-thrust belt. Earth Planet. Sci. Lett. 205, 13–24.
Davydov, V.I., Crowley, J.L., Schmitz, M.D., Poletaev, V.I., 2010. High-precision U-Pb zircon age calibration of the global Carboniferous time scale and Milankovitch band cyclicity in the Donets basin, eastern Ukraine. Geochem. Geophys. Geosyst. 11 (2).
Deng, X.Q., Luo, A.X., Zhang, Z.Y., Liu, X., 2013. Geochronological comparison on Indosinian tectonic events between Qinling Orogeny and Ordos Basin. Acta Sedimentol. Sin. 31, 939–953 (in Chinese with English abstract).
Deng, S., Lu, Y., Luo, Z., Fan, R., Li, X., Zhao, Y., Ma, X., Zhu, R., Cui, J., 2018. Subdivision and age of the Yanchang Formation and the Middle/Upper Triassic boundary in Ordos Basin, North China. Sci. China Earth Sci. 61, 1419–1439.
Dong, Y., Zhang, X., Liu, X., Li, W., Chen, Q., Zhang, G., Zhang, H., Yang, Z., Sun, S., Zhang, F., 2015. Propagation tectonics and multiple accretionary processes of the Qinling Orogen. J. Asian Earth Sci. 104, 84–98.
Escudero-Mozo, M.J., Márquez-Aliaga, A., Goy, A., Martín-Chivelet, J., López-Gómez, J., Márquez, L., Arche, A., Plasencia, P., Marzo, M., Sánchez-Fernández, D., 2015. Middle Triassic carbonate platforms in eastern Iberia: evolution of their fauna and palaeogeographic significance in the western Tethys. Palaeogeogr. Palaeoclimatol. Palaeoecol. 417, 236–260.
Franz, M., Kaiser, S.I., Fischer, J., Heunisch, C., Kustatscher, E., Luppold, F.W., Berner, U., Röhling, H.G., 2015. Eustatic and climatic control on the Upper Muschelkalk Sea (late Anisian/Ladinian) in the Central European Basin. Glob. Planet. Chang. 135, 1–27.
Gao, Y., Jiang, Z., Best, J.L., Zhang, J., 2020. Soft-sediment deformation structures as indicators of tectono-volcanic activity during evolution of a lacustrine basin: a case study from the Upper Triassic Ordos Basin, China. Mar. Pet. Geol. 115, 104250.
Gerstenberger, H., Haase, G.A., 1997. Highly effective emitter substance for mass spectrometric Pb isotope ratio determinations. Chem. Geol. 136, 309–312.
Gianolla, P., Jacquin, T., 1998. Triassic sequence stratigraphic framework of Western European basins. In: de Graciansckcy, P.C., Hardenbol, J., Jacquin, T., Vail, P.R., Ulmer-Scholle, D. (Eds.), Mesozoic-Cenozoic Sequence Stratigraphy of European Basins, SEPM Special Publication, vol. 60, pp. 643–650.
Gianolla, P., De Zanche, V., Mietto, P., 1998. Triassic sequence stratigraphy in the Southern Alps. Definition of sequences and basin evolution. In: de Graciansckcy, P.C., Hardenbol, J., Jacquin, T., Vail, P.R., Ulmer-Scholle, D. (Eds.), Mesozoic-Cenozoic Sequence Stratigraphy of European Basins, 60. SEPM Special Publication, pp. 723–751.
Gianolla, P., Caggiati, M., Riva, A., 2021. The interplay of carbonate systems and volcanics: cues from the 3D model of the Middle Triassic Sciliar/Schlern platform (Dolomites, Southern Alps). Mar. Pet. Geol. 124, 104794.
Golonka, J., 2007. Late Triassic and early Jurassic palaeogeography of the world. Palaeogeogr. Palaeoclimatol. Palaeoecol. 244, 297–307.
Guo, Y.Q., Hui, L., Zhang, X.N., Wei, Q.S., Li, W.H., Li, B.Q., 2018. Sedimentary system characteristics and lake basin evolution of Triassic Yanchang Formation in Ordos Basin. J. Northwest Univ. 48, 593–602 (in Chinese with English abstract).
Haq, B.U., 2018. Triassic eustatic variations reexamined. GSA Today 28, 4–9.
Hardenbol, J., Thierry, J., Farley, M.B., Jacquin, T., De Graciansky, P.C., Vail, P.R., 1998. Mesozoic and Cenozoic sequence chronostratigraphic framework of European basins. In: de Graciansky, P.C., et al. (Eds.), Mesozoic and Cenozoic Sequence Stratigraphy of European Basins, 60. eSEPM Special Publication, pp. 3–13.
Helby, R., Morgan, R., Partridge, A.D., 1987. A palynological zonation of the Australian Mesozoic. Mem. Assoc. Austral. Palaeontol. 4, 1–94.
Hornung, T., Brandner, R., Krystyn, L., Joachimski, M.M., Keim, L., 2007. Multistratigraphic Constraints on the NW Tethyan "Carnian Crisis", 4. New Mexico Museum of Natural History and Science, pp. 9–67.
Ilyina, N.V., Egorov, A.Y., 2008. The Upper Triassic of northern Middle Siberia: stratigraphy and palynology. Polar Res. 27, 372–392.
Jacobson, G.L., Bradshaw, R.H.W., 1981. The selection of sites for palaeovegetational studies. Quat. Res. 16, 80–96.
Jaffey, A.H., Flynn, K.F., Glendenin, L.E., Bentley, W.T., Essling, A.M., 1971. Precision measurement of half-lives and specific activities of $U^{235}$ and $U^{238}$. Phys. Rev. C 4, 1889.
Jaramillo, C.A., Oboh-Ikuenobe, F.E., 1999. Sequence stratigraphic interpretations from palynofacies, dinocyst and lithological data of Upper Eocene–Lower Oligocene strata in southern Mississippi and Alabama, U.S. Gulf Coast. Palaeogeogr. Palaeoclimatol. Palaeoecol. 145, 259–302.
Ji, L.M., Meng, F., 2006. Palynology of Yanchang Formation of Middle and Late Triassic in Eastern Gansu Province and its Paleoclimatic significance. J. China Univ. Geosci. 17, 209–220.
Ji, L.M., Zhu, Y., 2013. Sporo-pollen assemblages and paleoclimate of the Yanchang Formation in the Xifeng area southwestern Ordos Basin, Gansu province, NW China. Acta Micropalaeontol. Sin. 30, 367–378 (in Chinese with English abstract).
Ji, L.M., Wang, S.F., Xu, J.L., 2006. Acritarch assemblage in Yanchang Formation in eastern Gansu province and its environmental implications. Earth Sci. 31, 789–807 (in Chinese with English abstract).
Ji, L.M., Wu, T., Li, L.T., 2007. Geochemical characteristics of kerogen in Yanchang Formation source rocks, Xifeng area, Ordos Basin. Pet. Explor. Dev. 34, 424 (in Chinese with English abstract).
Ji, L.M., Yan, K., Meng, F.W., Zhao, M., 2010. The oleaginous Botryococcus from the Triassic Yanchang Formation in Ordos Basin, northwestern China: morphology and its paleoenvironmental significance. J. Asian Earth Sci. 38, 175–185.
Korte, C., Kozur, H.W., Veizer, J., 2005. $\delta^{13}C$ and $\delta^{18}O$ values of Triassic brachiopods and carbonate rocks as proxies for coeval seawater and palaeotemperature. Palaeogeogr. Palaeoclimatol. Palaeoecol. 226, 287–306.
Krogh, T.E., 1973. A low contamination method for hydrothermal decomposition of zircon and extraction of U and Pb for isotopic age determinations. Geochim. Cosmochim. Acta 37, 485–494.
Kürschner, W.M., Herngreen, G.F.W., 2010. Triassic palynology of central and northwestern Europe: a review of palynofloral diversity patterns and biostratigraphic subdivisions. Geol. Soc. Lond., Spec. Publ. 334, 263–283.
Kustatscher, E., van Konijnenburg-van Cittert, J.H.A., Roghi, G., 2010. Macrofloras and palynomorphs as possible proxies for palaeoclimatic and palaeoecological studies: a case study from the Pelsonian (Middle Triassic) of Kühwiesenkopf/Monte Prà della Vacca (Olang Dolomites, N-Italy). Palaeogeogr. Palaeoclimatol. Palaeoecol. 290, 71–80.
Kustatscher, E., Heunisch, C., van Konijnenburg-van Cittert, J.H.A., 2012a. Taphonomical implications of the Ladinian megaflora and palynoflora of Thale (Germany). Palaios 27, 753–764.
Kustatscher, E., Kelber, K.-P., van Konijnenburg-van Cittert, J.H.A., 2012b. *Danaeopsis* Heer ex Schimper 1869 and its European Triassic species. Rev. Palaeobot. Palynol. 183, 32–49.
Li, S., Xiao, Y., Liou, D., Chen, Y., Ge, N., Zhang, Z., Sun, S., Cong, B., Zhang, R., Hart, S., Wang, S., 1993. Collision of the North China and Yangtse Blocks and formation of coesite-bearing eclogites: timing and processes. Chem. Geol. 109, 89–111.
Li, L., Wang, Y., Liu, Z., Zhou, N., Wang, Y., 2016. Late Triassic palaeoclimate and palaeoecosystem variations inferred by palynological record in the northeastern Sichuan Basin, China. PalZ 90, 327–348.
Li, Q., Wu, S., Xia, D., You, X., Zhang, H., Lu, H., 2020. Major and trace element geochemistry of the lacustrine organic-rich shales from the Upper Triassic Chang 7 Member in the southwestern Ordos Basin, China: implications for paleoenvironment and organic matter accumulation. Mar. Pet. Geol. 111, 852–867.
Lin, S., Yuan, X., Tao, S., Yang, Z., Wu, S., 2013. Geochemical characteristics of the source rocks in Mesozoic Yanchang Formation, central Ordos Basin. J. Earth Sci. 24, 804–814.
Lin, W., Chen, L., Lu, Y., Hu, H., Liu, L., Liu, X., Wei, W., 2017. Diagenesis and its impact on reservoir quality for the Chang 8 oil group tight sandstone of the Yanchang Formation (upper Triassic) in southwestern Ordos basin, China. J. Petrol. Explor. Product. Technol. 7, 947–959.
Lindström, S., Erlström, M., Piasecki, S., Nielsen, L.H., Mathiesen, A., 2017. Palynology and terrestrial ecosystem change of the Middle Triassic to lowermost Jurassic succession of the eastern Danish Basin. Rev. Palaeobot. Palynol. 244, 65–95.
Liu, X.T., 1962. Two new hybodus from North Shensi, China. Vertebr. PalAsiatica 6, 150–156 (in Chinese with English abstract).
Liu, B.P., Li, Z.S., 1980. Bivalvia fossils. In: IGCAGS (Ed.), Mesozoic Stratigraphy and Palaeontology of Ordos Basin (2). Geological Publishing House, Beijing, pp. 1–47.
Liu, S., Yang, S., 2000. Upper Triassic–Jurassic sequence stratigraphy and its structural controls in the western Ordos Basin, China. Basin Res. 12, 1–18.
Liu, Z.S., Shang, Y.K., Li, W.B., 1981. Triassic and Jurassic Spore-pollen Assemblages From Some Localities of Shaanxi and Gansu, North-West China, 3. Bulletin of Nanjing Institute of Geology and Palaeontology, Chinese Academy of Sciences, pp. 131–210 (in Chinese with English abstract).
Liu, G.B., Zhu, Z.X., Zhang, X.L., 1999. A coelacanthid fossil from Huachi area, Gansu Province. Geol. J. China Univ. 5, 474–480 (in Chinese with English abstract).
Liu, S., Su, S., Zhang, G., 2013. Early Mesozoic basin development in North China: Indications of cratonic deformation. J. Asian Earth Sci. 62, 221–236.
Liu, F., Zhu, X., Li, Y., Xu, L., Niu, X., Zhu, S., Liang, X., Xue, M., He, J., 2015. Sedimentary characteristics and facies model of gravity flow deposits of Late Triassic Yanchang Formation in southwestern Ordos Basin, NW China. Pet. Explor. Dev. 42, 633–645.
Mattinson, J.M., 2005. Zircon U–Pb chemical abrasion ("CA-TIMS") method: combined annealing and multi-step partial dissolution analysis for improved precision and accuracy of zircon ages. Chem. Geol. 220, 47–66.
McLean, N.M., Condon, D.J., Schoene, B., Bowring, S.A., 2015. Evaluating uncertainties in the calibration of isotopic reference materials and multi-element isotopic tracers (EARTHTIME Tracer Calibration Part II). Geochim. Cosmochim. Acta 164, 481–501.
Mendonça Filho, J.G., Menzes, T.R., de Oliveira Mendonça, J., 2011. Chapter 5: Organic Composition (Palynofacies Analysis). ICCP Training Course on Dispersed Organic Matter, pp. 1–54.
Mendonça Filho, J.G., Menezes, T.R., Mendonça, J.O., Oliveira, A.D., Silva, T.F., Rondon, N.F., Silva, F.S., 2012. Organic facies: palynofacies and organic geochemistry approaches. In: Panagiotaras, D. (Ed.), Geochemistry - Earth's System Processes. InTech, Rijeka, pp. 211–248.
Meyers, P.A., 1994. Preservation of elemental and isotopic source identification of sedimentary organic matter. Chem. Geol. 114, 289–302.
Mietto, P., Manfrin, S., 1995. A high resolution Middle Triassic ammonoid standard scale in the Tethys realm; a preliminary report. Bull. Geol. Soc. France 166, 539–563.
Mietto, P., Manfrini, S., Preto, N., Rigo, M., Roghi, G., Furin, S., Gianolla, P., Posenato, R., Muttoni, G., Nicora, A., Buratti, N., Cirilli, S., Spötl, C., Ramezani, J., Bowring, S.A., 2012. The Global Boundary Stratotype Section and Point (GSSP) of the Carnian Stage (Late Triassic) at Prati di Stuores/Stuores Wiesen Section (Southern Alps, NE Italy). Episodes 35, 414–430.

Oboh-Ikuenobe, F.E., Yepes, O., Gregg, J.M., 1998. Palynostratigraphy, palynofacies, and thermal maturation of Cretaceous-Paleogene sediments from the Côte D'Ivoire-Ghana transform margin. In: Proc Ocean Drill Prog Scient Res, Vol. 159, pp. 277–318.
Ogg, J.G., Chen, Z.Q., Orchard, M.J., Jiang, H.S., 2020. The triassic period. In: Geologic Time Scale 2020. Elsevier, pp. 903–953.
Paterson, N.W., Mangerud, G., 2019. A revised palynozonation for the Middle–Upper Triassic (Anisian–Rhaetian) series of the Norwegian Arctic. Geol. Mag. 157, 1568–1592.
Paterson, N.W., Mangerud, G., Mørk, A., 2017. Late Triassic (early Carnian) palynology of shallow stratigraphical core 7830/5-U-1, offshore Kong Karls Land, Norwegian Arctic. Palynology 41, 230–254.
Peng, J., Li, J., Li, W., Slater, S.M., Zhu, H., Vajda, V., 2018. The Triassic to Early Jurassic palynological record of the Tarim Basin, China. Palaeobiodivers. Palaeoenviron. 98, 7–28.
Preto, N., Spötl, C., Guaiumi, C., 2009. Evaluation of bulk carbonate $\delta^{13}C$ data from Triassic hemipelagites and the initial composition of carbonate mud. Sedimentology 56, 1329–1345.
Qiu, X., Liu, C., Mao, G., Deng, Y., Wang, F., Wang, J., 2014. Late Triassic tuff intervals in the Ordos basin, Central China: their depositional, petrographic, geochemical characteristics and regional implications. J. Asian Earth Sci. 80, 148–160.
Qu, L.F., 1980. Triassic spores and pollen. In: IGCAGS (Ed.), Mesozoic Stratigraphy and Palaeontology of Ordos Basin (1). Geological Publishing House, Beijing, pp. 115–204 (in Chinese with English abstract).
Qu, L.F., Yang, J.D., Bai, Y.H., Zhang, Z.L., 1983. A preliminary discussion on the characteristics and stratigraphic division of Triassic spores and pollen in China. Bull. Chin. Acad. Geol. Sci. 5, 81–94 (in Chinese with English abstract).
Ritts, B.D., Hanson, A.D., Darby, B.J., Nanson, L., Berry, A., 2004. Sedimentary record of Triassic intraplate extension in North China: evidence from the nonmarine NW Ordos Basin, Helan Shan and Zhuozi Shan. Tectonophysics 386, 177–202.
Roghi, G., 2004. Palynological investigations in the Carnian of the Cave del Predil area (Julian Alps, NE Italy). Rev. Palaeobot. Palynol. 132, 1–35.
Rovnina, L.V., 1973. Development of Flora During the Early Mesozoic in Western Siberia and Its Possible Relationships With Synchronous Floras of Some Other Regions. Palynology of Mesophyte, Moscow, pp. 38–41 (in Russian).
Sakulina, G.V., 1973. Middle and Late Triassic Miospores From Southeastern Kazakhstan. Palynology of Mesophyte, Moscow, pp. 33–38 (in Russian).
Schmitz, M.D., Davydov, V.I., 2012. Quantitative radiometric and biostratigraphic calibration of the Pennsylvanian–Early Permian (Cisuralian) time scale and pan-Euramerican chronostratigraphic correlation. Geol. Soc. Am. Bull. 124, 549–577.
Schmitz, M.D., Schoene, B., 2007. Derivation of isotope ratios, errors, and error correlations for U-Pb geochronology using $^{205}Pb$-$^{235}U$-($^{233}U$)-spiked isotope dilution thermal ionization mass spectrometric data. Geochem. Geophys. Geosyst. 8 (8).
Scotese, C.R., 2014. Atlas of Middle & Late Permian and Triassic Paleogeographic Maps, Maps 43–48 From Volume 3 of the PALEOMAP Atlas for ArcGIS (Jurassic and Triassic) and Maps 49–52 from Volume 4 of the PALEOMAP PaleoAtlas for ArcGIS (Late Paleozoic). Mollweide Projection, PALEOMAP Project, Evanston, IL.
Shang, Y.K., 1998. Late Triassic palynoflora provinces of China. Acta Palaeontol. Sin. 37, 427–445 (in Chinese with English abstract).
Silva, R.L., Mendonça Filho, J.G., Azerêdo, A.C., Duarte, L.V., 2014. Palynofacies and TOC analysis of marine and non-marine sediments across the Middle-Upper Jurassic boundary in the central-northern Lusitanian Basin (Portugal). Facies 60, 255–276.
Su, D.Y., Li, Y.G., Pang, Q.Q., Chen, S.E., 1980. Ostracod fossils. In: IGCAGS (Ed.), Mesozoic Stratigraphy and Palaeontology of Ordos Basin (2). Geological Publishing House, Beijing, pp. 48–83 (in Chinese with English abstract).
Sun, Z., Xie, Q., Yang, J., 1989. Ordos Basin—a typical example of an unstable cratonic interior superimposed basin. In: Zhu, X. (Ed.), Chinese Sedimentary Basins. Elsevier, New York, pp. 63–75.
Sun, Y., Li, X., Liu, Q., Zhang, M., Li, P., Zhang, R., Shi, X., 2020. In search of the inland Carnian Pluvial Event: Middle–Upper Triassic transition profile and U–Pb isotopic dating in the Yanchang Formation in Ordos Basin, China. Geol. J. 55, 4905–4919.
Țabără, D., Pacton, M., Makou, M., Chirilă, G., 2015. Palynofacies and geochemical analysis of Oligo-Miocene bituminous rocks from the Moldavidian Domain (Eastern Carpathians, Romania): implications for petroleum exploration. Rev. Palaeobot. Palynol. 216, 101–122.
Talbot, M.R., 1988. The origins of lacustrine oil source rocks: evidence from the lakes of tropical Africa. Geol. Soc. Lond., Spec. Publ. 40, 29–43.
Trotter, J.A., Williams, I.S., Nicora, A., Mazza, M., Rigo, M., 2015. Long-term cycles of Triassic climate change: a new $\delta^{18}O$ record from conodont apatite. Earth Planet. Sci. Lett. 415, 165–174.
Tverdokhlebov, V.P., Sennikov, A.G., Novikov, I.V., Ilyina, N.V., 2020. The youngest Triassic land vertebrate assemblage of Russia: composition and dating. Paleontol. J. 54, 297–310.
Tyson, R.V., 1995. Palynological Kerogen Classification. In: Sedimentary Organic Matter. Springer, Dordrecht, pp. 341–365.
Wang, S.E., Liu, S.W., 1980. Conchostraca fossils. In: IGCAGS (Ed.), Mesozoic Stratigraphy and Palaeontology of Ordos Basin (2). Geological Publishing House, Beijing, pp. 84–110 (in Chinese with English abstract).
Wang, D., Xin, B., Yang, H., Fu, J., Yao, J., Zhang, Y., 2014. Zircon SHRIMP U-Pb age and geological implications of tuff at the bottom of Chang-7 Member of Yanchang Formation in the Ordos Basin. Sci. China Earth Sci. 57, 2966–2977.
Wang, J.Q., Liu, C.Y., Li, H., Wu, T.T., Wu, J.L., 2017a. Geochronology, potential source and regional implications of tuff intervals in Chang-7 Member of Yanchang Formation, South of Ordos Basin. Acta Sedimentol. Sin. 35, 691–704 (in Chinese with English abstract).
Wang, C., Wang, Q., Chen, G., He, L., Xu, Y., Chen, L., Chen, D., 2017b. Petrographic and geochemical characteristics of the lacustrine black shales from the Upper Triassic Yanchang Formation of the Ordos Basin, China: implications for the organic matter accumulation. Mar. Pet. Geol. 86, 52–65.
Wood, G.D., Gabriel, A.M., Lawson, J.C., 1996. Chapter 3. Palynological techniques – processing and microscopy. In: Jansonius, J., McGregor, D.C. (Eds.), Palynology: Principles and Applications, 1. American Association of Stratigraphic Palynologists Foundation, Dallas, pp. 29–50.
Wotzlaw, J.F., Brack, P., Storck, J.C., 2018. High-resolution stratigraphy and zircon U–Pb geochronology of the Middle Triassic Buchenstein Formation (Dolomites, northern Italy): precession-forcing of hemipelagic carbonate sedimentation and calibration of the Anisian–Ladinian boundary interval. J. Geol. Soc. 175, 71–85.
Xu, W., Ruhl, M., Jenkyns, H.C., Hesselbo, S.P., Riding, J.B., Selby, D., Naafs, D., Weijers, J., Pancost, R., Tegelaar, E., Idiz, E.F., 2017. Carbon sequestration in an expanded lake system during the Toarcian oceanic anoxic event. Nat. Geosci. 10, 129–134.
Xu, W., Weijers, J.W., Ruhl, M., Idiz, E.F., Jenkyns, H.C., Riding, J.B., Gorbanenko, O., Hesselbo, S.P., 2021. Molecular and petrographical evidence for lacustrine environmental and biotic change in the palaeo-Sichuan mega-lake (China) during the Toarcian Oceanic Anoxic Event. Geol. Soc. Lond., Spec. Publ. 514.
Yan, Y., Zhao, Q., Zhang, Y., Huang, B., Zheng, W., Zhang, P., 2019. Direct paleomagnetic constraint on the closure of Paleo-Tethys and its implications for linking the Tibetan and Southeast Asian Blocks. Geophys. Res. Lett. 46, 14368–14376.
Yang, H., Deng, X.Q., 2013. Deposition of Yanchang formation deep-water sandstone under the control of tectonic events, Ordos basin. Pet. Explor. Dev. 40, 513–520.
Yang, Y., Li, W., Ma, L., 2005. Tectonic and stratigraphic controls of hydrocarbon systems in the Ordos basin: a multicycle cratonic basin in Central China. AAPG Bull. 89, 255–269.
Yang, W.W., Liu, G.D., Liu, X.Y., 2013. The accumulation mechanism and accumulation models of oil in low permeability reservoir of Yanchang Formation in Longdong area, Ordos basin. Front. Earth Sci. 20, 132–139 (in Chinese with English abstract).
Yang, R., Jin, Z., Van Loon, A.J., Han, Z., Fan, A., 2017. Climatic and tectonic controls of lacustrine hyperpycnite origination in the Late Triassic Ordos Basin, Central China: implications for unconventional petroleum development. AAPG Bull. 101, 95–117.
Zhang, Z.H., Fu, Z.Y., Luo, K.Q., et al., 1982. Mesozoic sporopollen assemblages from the Southern Shaan-Gan-Ning Basin. In: Selected Works of the First Academic Meeting of Sporopollen Society of China. Science Press, Beijing, pp. 116–124 (in Chinese with English abstract).
Zhang, H., Peng, P.A., Zhang, W.Z., 2014. Zircon U-Pb ages and Hf isotope characterization and their geological significance of Chang 7 tuff of Yanchang Formation in Ordos basin. Acta Petrol. Sin. 30, 565–575 (in Chinese with English abstract).
Zhang, M., Ji, L., Wu, Y., He, C., 2015. Palynofacies and geochemical analysis of the Triassic Yanchang Formation, Ordos Basin: implications for hydrocarbon generation potential and the paleoenvironment of continental source rocks. Int. J. Coal Geol. 152, 159–176.
Zhang, Y.P., Chen, X.H., Zhang, J., Shao, Z.G., Ding, W.C., Guo, X.G., Wang, D.R., Gu, W. P., Wang, Y., Xu, S.L., Qin, X., 2019a. Discussion on the initial timing of the Indosinian movement in the Ordos basin and the Sichuan basin: constraints from growth strata evidence. Geol. China 46, 1021–1038 (in Chinese with English abstract).
Zhang, R., Jin, Z., Liu, Q., Li, P., Huang, Z., Shi, J., Ge, Y., Du, K., 2019b. Astronomical constraints on deposition of the Middle Triassic Chang 7 lacustrine shales in the Ordos Basin, Central China. Palaeogeogr. Palaeoclimatol. Palaeoecol. 528, 87–98.
Zhu, R., Cui, J., Deng, S., Luo, Z., Lu, Y., Qiu, Z., 2019. High-precision dating and geological significance of Chang 7 tuff zircon of the Triassic Yanchang Formation, Ordos Basin in Central China. Acta Geol. Sin. 93, 1823–1834.
Zou, C.N., Zhang, X.Y., Luo, P., Wang, L., Luo, Z., Liu, L.H., 2010. Shallow-lacustrine sand-rich deltaic depositional cycles and sequence stratigraphy of the Upper Triassic Yanchang Formation, Ordos Basin, China. Basin Res. 22, 108–125.